AIAA JOURNAL
Vol. 36, No. 7, July 1998

Experimental Investigation of Unsteady Aerodynamics and Aeroacoustics of a Thin Airfoil

R. J. Minniti III* and T. J. Mueller†
University of Notre Dame, Notre Dame, Indiana 46556

An experimental investigation of the unsteady problem for a thin, symmetric airfoil exposed to periodic gusting was performed in a free-jet anechoic wind-tunnel facility. The gusting events were created upstream such that there was a small longitudinal, i.e., spanwise, wave number and the gust could be approximated as two dimensional. Measurements of the unsteady velocity field, the unsteady pressure at the airfoil surface, and the acoustic field were made for two values of axial and normal reduced frequency. The unsteady pressure distribution along the airfoil was computed using the Sears method and unsteady velocity data. In addition, the pressure distribution was computed using acoustic data as input to a numerical inversion technique. The results of each technique were compared with the experimentally obtained unsteady pressure distribution. The inversion technique showed good agreement with the Sears method. However, comparison with experimental results illustrated that the theoretical estimates, although exhibiting trends similar to the experimental data, consistently underestimated the experimental unsteady pressure distribution at the lower reduced frequency, indicating the presence of viscous effects. Better agreement between experimental and theoretical results was obtained at the higher reduced frequency where viscous effects were less prominent.

Nomenclature

$\boldsymbol{a}$	= gust velocity vector
$C_{p'}$	= unsteady pressure coefficient, $p'/\rho a_2 U_\infty$
c	= airfoil chord
f_k	= single discrete value within the frequency range of spectral analysis
f_{RPF}	= primary rod passage frequency
$H_v^{(2)}$	= vth-order Hankel function of the second kind
K	= Helmholtz operator
$\boldsymbol{k}$	= wave number vector
M_∞	= freestream Mach number
m	= harmonic (mode) number
$P(\boldsymbol{y})$	= acoustic pressure measured at observation location
$S(k_1)$	= Sears function
$U(t)$	= axial velocity component
$\boldsymbol{U}(\boldsymbol{x}, t)$	= total velocity field
$\boldsymbol{U}_D$	= velocity deficit in stationary frame
$\boldsymbol{U}_G$	= gust velocity vector
$\boldsymbol{U}_m$	= velocity deficit in wake behind the rod
$\boldsymbol{U}_R$	= rotational velocity of rod
$\boldsymbol{U}_0$	= relative velocity seen by rotating rod
$\boldsymbol{U}_\infty$	= freestream velocity vector
$\boldsymbol{u}(\boldsymbol{x}, t)$	= unsteady portion of velocity field
$\boldsymbol{u}_a(\boldsymbol{x}, t)$	= acoustic portion of unsteady velocity
$\boldsymbol{u}_\infty(\boldsymbol{x}, t)$	= rotational portion of unsteady velocity
$V(t)$	= normal velocity component
$\boldsymbol{x}$	= source position vector
$\boldsymbol{y}$	= acoustic field observation position vector
$\Delta p'(x_1^*, k_1^*)$	= unsteady pressure jump on airfoil
ρ	= density of air
ω	= gust frequency

Subscripts

1	= scalar component of a vector parallel to freestream
2	= scalar component of a vector normal to airfoil planform
3	= scalar component of a vector parallel to span of airfoil

Superscript

*	= nondimensional quantity

Introduction

MANY airfoils, hydrofoils, and propulsive system structural components operate in nonuniform or unsteady inflow conditions. Nonuniformity and unsteadiness are caused by a variety of sources, including wakes, secondary flows, and turbulence. The transient interaction of a body with an approaching flow disturbance, typically termed a gust, causes unsteady aerodynamic or hydrodynamic loading. This unsteady loading is important not only because of the energy losses and induced vibrations but also for its role in the generation of sound. To date, most research into unsteady problems has dealt with rotor–stator interactions, air and marine propellers, and helicopter rotors. These represent the most common situations where periodic, transient interactions occur between flows and aerodynamic bodies producing large amounts of acoustic radiation. The experiments and numerical simulations used to investigate these situations often involve very complex flowfields accompanied by complex physical geometries. Consequently, many simplifying assumptions are made in dealing with these unsteady problems.

Treatment of the unsteady problem for aerodynamic bodies can be split into two parts. The first is the aerodynamic problem associated with the production of unsteady lift on the body by transient interaction with incoming unsteady velocities. The second part of the unsteady problem is the aeroacoustic problem associated with the acoustic production of the airfoil due to gust interaction. Each of these problems has been solved by direct theoretical methods that infer the unsteady lift on the airfoil from the incoming flow quantities and then project the acoustic far field from the unsteady lift. Additionally, inverse theoretical solutions to the problems have been developed to infer the unsteady lift from the acoustic field and then predict the incoming flowfield from the unsteady lift.

The current work experimentally investigates the direct aerodynamic and inverse aeroacoustic solutions for the thin, symmetric airfoil in unsteady flow. As such, two independent estimates of

Received Aug. 17, 1997; revision received March 23, 1998; accepted for publication March 23, 1998.

*Research Associate, Department of Aerospace and Mechanical Engineering; currently Mechanical Engineer, Signatures Directorate Code 7250, David Taylor Model Basin, U.S. Naval Surface Warfare Center, Carderock Division, 9500 MacArthur Boulevard, West Bethesda, MD 20817-5700.

†Roth-Gibson Professor, Department of Aerospace and Mechanical Engineering, 365 Fitzpatrick Hall. Associate Fellow AIAA.

the unsteady pressure distribution along the chord of the airfoil were made based on experimental data and two different theoretical techniques. In the first instance, the distribution was estimated from measurements of the unsteady velocity field and the classical development of Sears.[1] The second estimate was made based on experimental measurements of the acoustic field and an inversion technique developed by Grace et al.[2] The two independent developments were then compared with direct measurements of the unsteady pressure distribution made at the airfoil surface.

Theoretical Development

To more clearly understand the experimental quantities of interest and their relationship to each other, a brief statement of the theoretical treatment of both the aerodynamic and aeroacoustic solutions for a thin airfoil is given. More complete discussions of the theoretical development are given by Sears,[1] von Kármán and Sears,[3] Atassi,[4] and Atassi et al.[5]

The equations governing an inviscid, compressible flow past an airfoil at zero angle of attack to a stream with uniform upstream velocity $\boldsymbol{U}_\infty$ are the Euler equations. If it is assumed that the unsteady flow component is small, then the upstream flow can be linearized about the mean flow as

$$\boldsymbol{U}(\boldsymbol{x}, t) = U_\infty \boldsymbol{i}_1 + \boldsymbol{u}_\infty(\boldsymbol{x} - \boldsymbol{i}_1 U_\infty t) + \boldsymbol{u}_a(\boldsymbol{x}, t) \tag{1}$$

where the unsteady part of the flow is split into a rotational part $\boldsymbol{u}_\infty$ and an acoustic part $\boldsymbol{u}_a$. Additionally, changes in the density and pressure fields are assumed to be linear about the mean.

This linearization means $\boldsymbol{u}_\infty$ can be decomposed into its Fourier components and a single component can be considered without loss of generality. Thus the total velocity field for a single frequency component can be written as

$$\boldsymbol{U}(\boldsymbol{x}, t) = U_\infty \boldsymbol{i}_1 + \boldsymbol{a} \exp[i(\omega t - \boldsymbol{k} \cdot \boldsymbol{x})] + \boldsymbol{u}_a(\boldsymbol{x}, t) \tag{2}$$

with the continuity equation

$$\boldsymbol{a} \cdot \boldsymbol{k} = 0 \tag{3}$$

Using these assumptions, one can linearize the Euler equations to

$$\frac{\partial \rho'}{\partial t} + U_\infty \frac{\partial \rho'}{\partial x_1} + \nabla \cdot \boldsymbol{u}_a = 0 \tag{4}$$

$$\rho_0 \left(\frac{\partial \boldsymbol{u}_a}{\partial t} + U_\infty \frac{\partial \boldsymbol{u}_a}{\partial x_1} \right) = -\nabla p' \tag{5}$$

with the boundary conditions

$$u_{a_2}(x_1, 0, x_3) = -a_2 \exp[i(\omega t - \boldsymbol{k} \cdot \boldsymbol{x})] \tag{6}$$

for $-c/2 < x_1 < c/2$ and where p' and u_{a_2} are continuous in the wake where $x_1 > c/2$ and $x_2 = 0$.

Therefore, for an incompressible, two-dimensional gust, i.e., no spanwise reduced frequency, Sears[1] showed that the unsteady pressure distribution on a thin airfoil due to the normal component of the gust is given by

$$\Delta p'\left(x_1^*, k_1^*\right) = 2\rho_0 U_\infty \sqrt{\frac{1 - x_1^*}{1 + x_1^*}}\, a_2\left(k_1^*\right) S\left(k_1^*\right) \tag{7}$$

where

$$S\left(k_1^*\right) = \frac{2}{\pi k_1^* \left[H_0^{(2)}\left(k_1^*\right) - i H_1^{(2)}\left(k_1^*\right)\right]} \tag{8}$$

and location and wave number have been nondimensionalized by $c/2$. The nondimensional form of the wave number is typically referred to as the reduced frequency vector. The solution of Sears relies solely upon the magnitude of the normal gust and the axial reduced frequency. It does not account for the normal reduced frequency k_2^*, the axial gust amplitude a_1, or the distortion effects of steady loading.

The far field of $\Delta p'(x_1^*, k_1^*)$ represents the sound radiated from the plate and can be determined numerically based on the governing equations with appropriate terms included to allow compressibility effects. The numerical solvers yield the velocity and pressure fields accurately inside a computational domain that may extend several chord lengths from the airfoil. However, in most cases the numerical solutions break down in the outer limits of the computational domain because the magnitude of the unsteady velocity and pressure is on the order of machine precision.

In aeroacoustic applications, the computational solution domain is limited to the region of accuracy where the solver has recovered most of the characteristics of the freestream flow, i.e., outside of distortions in the freestream due to the presence of the body. At this limit, a Kirchhoff surface is introduced to the domain. Inside the surface, the pressure and velocity fields are established by the governing equations. Outside, the governing equations are reduced to the Helmholtz equation, and using Green's theorem, the far-field pressure is expressed in terms of its value at the Kirchhoff surface. However, in the case of an ideal flat plate, the mean flow is not distorted, and the problem is simplified by placing the Kirchhoff surface at the plate surface.

Atassi and Dusey[6] showed that by using Green's theorem the acoustic pressure for the thin airfoil could be expressed in terms of its value along the plate surface as

$$P(\boldsymbol{y}) = \frac{-i}{4} K y_2 \int_{-1}^{1} \Delta p'\left(x_1^*, k_1^*\right) \frac{H_1^{(2)}(K|\boldsymbol{x} - \boldsymbol{y}|)}{|\boldsymbol{x} - \boldsymbol{y}|}\, \mathrm{d}x_1^* \tag{9}$$

where $H_1^{(2)}$ represents Green's function of the Helmholtz equation whose constant is K. If it is assumed that the compressibility effects responsible for the acoustic production are small, Eq. (7) can be used to approximate the unsteady pressure distribution from the gust quantities. Equation (9) then establishes the subsequent acoustic field for the flat plate.

For this investigation, however, it was desired to calculate the unsteady surface pressure distribution along the airfoil surface from the far-field acoustic data. Therefore, it is necessary to invert Eq. (9) to solve for the pressure jump on the plate surface. The numerical solution of this inversion process is discussed in detail by Grace et al.[2] and is solved using a collocation technique and singular value decomposition. The set of basis functions, which expresses the pressure distribution, is chosen to match the Sears method in the limit of vanishing Mach number. The solution technique is dependent on the relative phase of the acoustic field recorded at different locations, as well as the magnitude and directivity of the far field.

Experimental Setup

The setup of the experiment is shown in Fig. 1 and was based on a similar experiment by Fujita and Kovasnay.[7] A thin, symmetric airfoil encountered an approximately two-dimensional, mean-gust pattern generated upstream by a rotating set of rods sweeping though the freestream flow of a free-jet, indraft wind tunnel. The thin airfoil completely spanned the flow of the free jet, and the wake generation

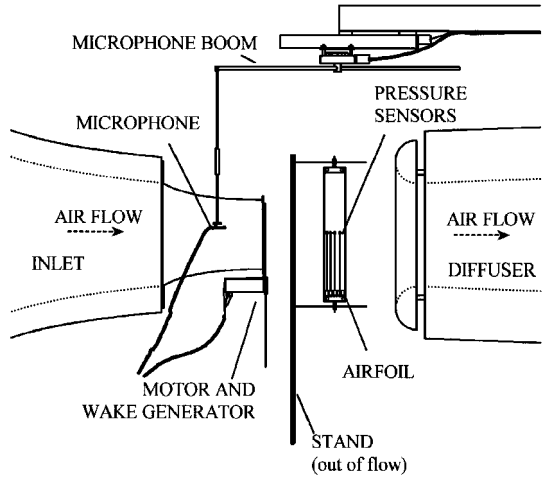

Fig. 1 Experimental setup used in investigation.

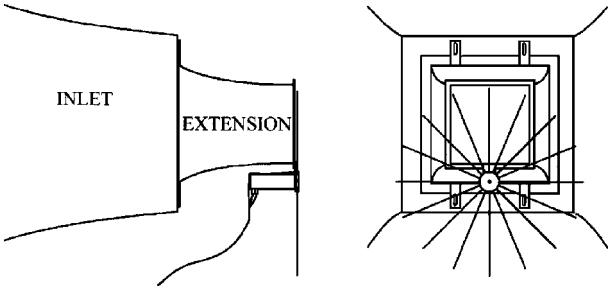

Fig. 2 Side and front views of wake generator on inlet face.

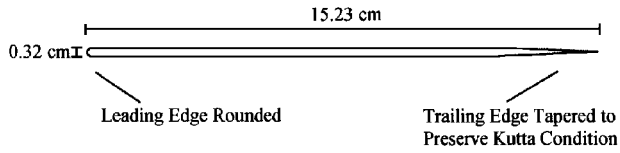

Fig. 3 Airfoil cross section.

device produced mean velocity distortions with components parallel to the mean flow and normal to the airfoil with a frequency and magnitude proportional to the rotational velocity.

The free jet had a 0.61×0.61 m cross section with a mean velocity range of 5–33 m/s and an undisturbed flow turbulence intensity level of 0.08% along the jet centerline one jet width downstream of the tunnel inlet. During the experiments, an extension was placed on the inlet, contracting the jet to 0.41×0.41 m. The extension increased the upper range of flow velocity to 40 m/s and reduced the turbulence intensity to 0.06%. The jet was housed inside an anechoic chamber, which provided an environment with very low background noise above the chamber's 100-Hz cutoff frequency. Such an environment was necessary for accurate measurement of the velocity, pressure, and acoustic fields. A complete description of the anechoic wind tunnel is given by Mueller et al.[8]

The periodic wake generator, shown in Fig. 2, was a pinwheel design that had a 130-cm diam and consisted of 16 circular cross-sectional rods of 6.35-mm diam each. It was mounted on the face of the tunnel extension exit such that the plane of the generator was 2.5 cm downstream of the exit. As seen in Fig. 2, two small sections at the top corners of the flowfield were not covered by the disk of the pinwheel due to limitations on the rod length by facility geometry. This meant that these sections of the flow were corrupted by end effects of the rod interacting with the jet and, therefore, were unusable during the experiments. Additionally, it was necessary to inspect the center of the upper section of the flowfield to ensure that these end effects did not corrupt the unsteady pressure distribution measured at the airfoil surface.

At the experimental rotational speed of 400 rpm, the Reynolds numbers based on rod diameter from the hub to the tip of the wake generator ranged from 8.2×10^3 to 1.23×10^4. At the midspan of the airfoil where the unsteady pressure measurements were taken, the Reynolds number was 1.025×10^4. This rotational speed resulted in a rod passage frequency of 107 Hz. The axial reduced frequency component was estimated to be 3.0 using the Taylor hypothesis, $k_1^* = \omega c/2U_\infty$.

The airfoil spanned the freestream flow at 30 cm (50 rod diameters) downstream of the wake generator along the jet centerline. The span of the airfoil extended beyond the limit of the free jet to avoid end effects on the unsteady flowfield. Additionally, the unsteady pressure measurements were made near the midspan of the airfoil with no sensor positioned more than 8% of the jet width from this location. The airfoil had a chord of 15.2 cm, a thickness of 3.175 mm, a rounded leading edge, and a tapered trailing edge; a cross-sectional view is shown in Fig. 3. The airfoil geometry was chosen to approximate an ideal flat plate, thus minimizing mean flow distortion and the effects of airfoil geometry on the system. During experiments the mean flow of the jet was set to 17 m/s, corresponding to a freestream Mach number of 0.05 and a Reynolds number based on the airfoil chord of 1.95×10^5.

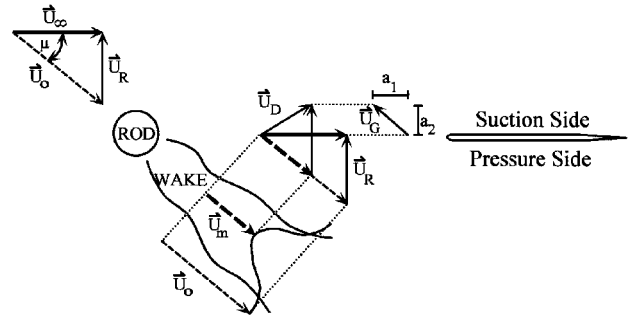

Fig. 4 Illustration of rod interacting with the freestream flow producing gust.

Describing the Unsteady Flowfield

Figure 4 shows the production of the gust components in the flowfield due to the shedding of the wake by the rotating rod for the special case when the rod is vertical and positioned directly upstream of the airfoil. The wake shed when the rod is in this position convects downstream to interact with the leading edge of the airfoil. At this point, the rotational velocity vector of the rod is normal to the airfoil along its entire length, which means that the wake that is produced will only have components parallel to the freestream and normal to the airfoil. When the rod is not vertical, its rotational velocity is not normal to the airfoil and thus produces a component along the span of the airfoil. However, this component is small compared with the other components as long as the rod is within 15 deg of vertical. Finally, the rotational velocity of the rod, and thus the magnitude of the normal component induced, increases linearly along its length. This means that there is variation in the gust along the span of the airfoil; however, the wavelength of this variation is much greater than the span of the airfoil, and thus the corresponding wave number is negligible in the experiments, allowing for treatment of the gust as two dimensional.

At the left in Fig. 4, the velocity seen by the rod, $\boldsymbol{U}_0$, is shown to be a combination of the rotational velocity of the rod $\boldsymbol{U}_R$ and the freestream velocity $\boldsymbol{U}_\infty$. The rod sheds a wake behind it, producing the mean velocity deficit shown in Fig. 4. The velocity $\boldsymbol{U}_m$ represents the minimum mean velocity behind the rod. In the center of the figure, the velocity components are returned to the stationary reference frame. With $\boldsymbol{U}_m$ superimposed upon $\boldsymbol{U}_0$, the gust production can be seen when $\boldsymbol{U}_R$ is removed. The undisturbed flow outside the wake simply recovers the freestream flow while the wake disturbance produces the vector $\boldsymbol{U}_D$. The gust velocity $\boldsymbol{U}_G$ is defined as the variation of the flow from the freestream; therefore, $\boldsymbol{U}_G$ is the resultant of $\boldsymbol{U}_\infty$ minus $\boldsymbol{U}_D$.

The wake shown in Fig. 4 is represented only by the mean flow distortion produced by the viscous interaction of the rod and the flow. The wake is actually composed of this mean distortion plus large-scale eddies formed by von Kármán–vortex shedding and small-scale turbulence. However, the leading edge of the airfoil is nearly 50 times the rod diameter downstream of the plane of the pinwheel. Thus, these components of the wake dissipate before reaching the leading edge, and the largest component of the remaining wake is the mean viscous distortion. Any remaining random portion of the wake will not necessarily be two dimensional or periodic. However, it accounts for a small portion of the unsteady energy as shown in the following sections.

Unsteady Flow Conditions

Velocity measurements were made at several locations in the flowfield to characterize the mean gust event encountered by the airfoil with a two-element, hot-wire probe. The locations included a spanwise and a normal series of measurements centered at the midspan of the airfoil and a grid of measurements in the plane normal to the airfoil midspan. The x wire measured the flow components parallel to the mean flow and normal to the airfoil directly in front of the leading edge of the airfoil. Probe calibration and conversion of raw data to velocity are covered in detail in Ref. 9. The uncertainty of the velocity data is given as ±2% of the reported value with 95% confidence.

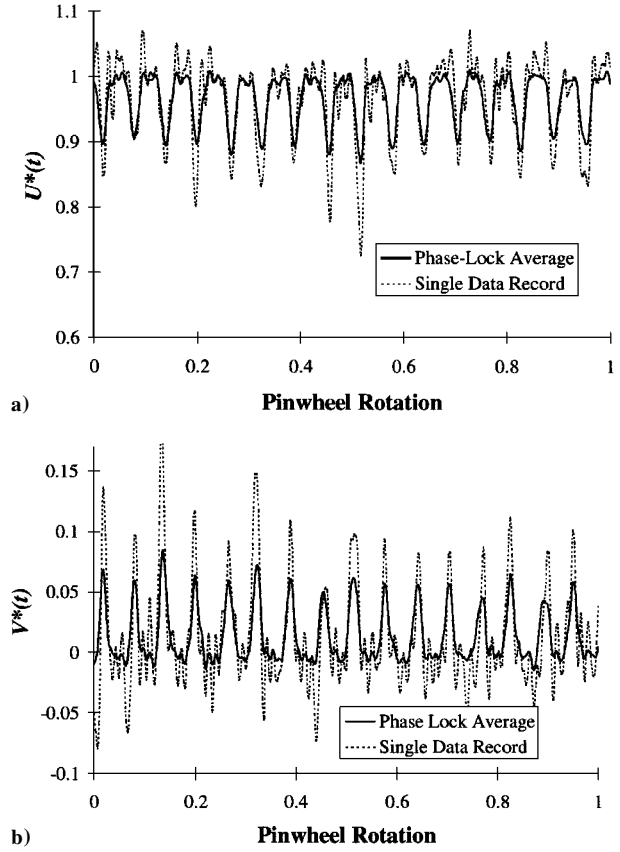

Fig. 5 a) Axial and b) normal velocity fluctuations at the jet center normalized by the freestream, 17 m/s (56 ft/s).

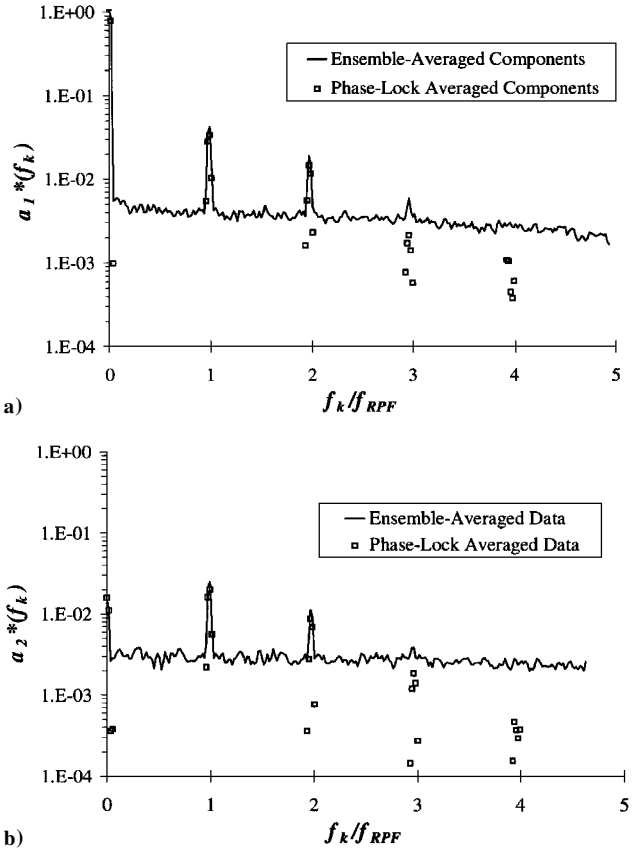

Fig. 6 Amplitude spectra of the a) axial and b) normal gust component at the jet center normalized by the freestream velocity, 17 m/s (56 ft/s).

The unsteady flow characteristics at the jet centerline were of primary importance, as this was the location where the unsteady pressure distribution was measured on the airfoil surface. To enable straightforward analysis in the time domain, the velocity components were phase lock averaged by triggering data acquisition on the position of the wake generator. Figure 5 compares the phase-lock average of the axial and normal velocity components nondimensionalized by the freestream velocity, $U^*(t)$ and $V^*(t)$, to single-data records. The comparison shows that the individual records are composed of large-scale gust events occurring at the rod passage frequency with random small-scale events superimposed. The phase-lock-averaging process has the effect of suppressing these smaller-scale events associated with freestream turbulence and viscous shedding of the rod. Aperiodicities remain in the phase-lock-averaged signal, which are symptomatic of rod-to-rod variations of the wakes, due to slight changes that have occurred over time due to wear and tear.

The same data can be described using spectral techniques for more quantitative analysis. Figure 6 shows the ensemble average of the gust component spectra computed from the x-wire data. Both signals are composed of the fundamental rod passage frequency and its second and third harmonics. The peaks are an order of magnitude above the broadband turbulence levels. Therefore, in much of the theoretical analysis each of the peaks in the spectrum is treated independently. Based on spectral analysis of the velocity measurements, the amplitude of the axial gust component associated with the rod passage frequency a_1 was 5.2% of the freestream velocity (0.9 m/s), and the normal gust component a_2 was 3.4% of the freestream velocity (0.6 m/s). The normal component in conjunction with Eq. (9) gives the theoretical pressure distribution along the airfoil obtained by Sears.

The spanwise series of measurements examined whether the character of the gust significantly changed within the region of measurement. The series of measurements extended 8 cm (3.1 in.) below and above the airfoil midspan, approximately 40% of the jet width. Figure 7 shows the phase-lock-averaged normal component measured at each of the spanwise locations translated by the spanwise

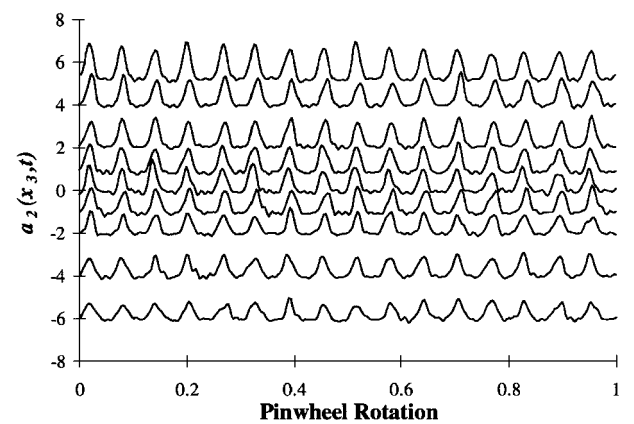

Fig. 7 Spanwise series of phase-lock-averaged normal gust component 2.5 cm (1.0 in.) upstream of the airfoil leading edge showing little phase variation along span.

measurement location to show the data clearly. Within this range of measurement, the axial component of the gust did not change, whereas the normal component varied linearly by 0.75% of the freestream velocity from the midspan value or about 23% of the normal component. The unsteady pressure measurements, however, were made within 1.5 cm (0.6 in.) of the midspan, and within this region the normal component varied from the midspan value by 0.2% of the freestream or 6% of the normal gust component. There is little phase variation of the gust along the span, again showing the spanwise wave number to be negligible.

The grid of measurements made normal to the airfoil established the unsteady gust field surrounding the airfoil. The measurements showed the variation of the two gust components in terms of magnitude and phase over a spatial range extending at least one chord length away from the airfoil surface in all directions. Mapping the magnitude and phase over the spatial domain enabled experimental

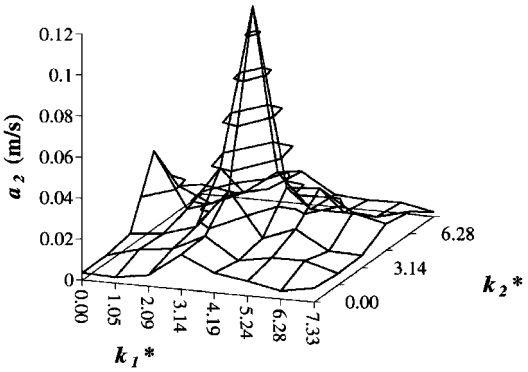

Fig. 8 Surface plot of the results of the two-dimensional wave-number analysis for the normal velocity component at the rod passage frequency, $a_2(k_1^*, k_2^*, f_{RPF})$.

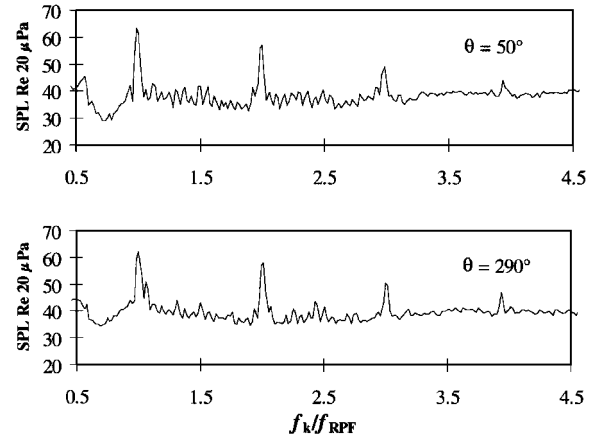

Fig. 9 Acoustical power spectra at circumferential locations around the airfoil.

resolution of the wave numbers associated with each gust component. The normal component of the reduced frequency vector can be estimated using the measured gust amplitudes and Eq. (3), giving $k_2^* = k_1^* |a_1/a_2| \approx 4.6$. This statement of continuity agrees with the geometrically defined wave number based on the spacing of the pinwheel rods at any radial location. Therefore, agreement of the empirical estimate with the physical geometry showed linear behavior of the gust production and justified the use of Taylor's hypothesis in estimating the axial component.

Figure 8 shows the result of a wave number analysis performed using velocity records taken over the grid in the plane normal to the airfoil span. A majority of the energy in the flow is associated with the rod passage frequency, concentrated at $(k_1^*, k_2^*) = (3.0, 4.6)$. The wave number analysis is covered in detail in Ref. 10, and the results show further justification for the use of Taylor's hypothesis and Eq. (3) to estimate the wave number components.

Acoustic Production

Information about the acoustic response of the airfoil was obtained using a 1.27-cm (0.5-in.) Brüel and Kjaer (B&K) microphone suspended from the end of a motorized boom centered above the airfoil, as shown in Fig. 1. By rotating the boom, the microphone was translated along a circular arc on either side of the airfoil with a radius of 25 times the half-chord. The arcs consisted of 26 measurement locations separated by 3 deg and thus covered a total of 75 deg on either side of the airfoil. The measurement location angle was defined by the mean freestream flow direction, with 0 deg being along the flow direction and 180 deg corresponding to the upstream direction. The measurements reported from 65 to 140 deg represent locations on the unsteady pressure side of the airfoil, whereas the measurements from 220 to 295 deg represent measurements made on the unsteady suction side of the airfoil.

The acoustic data were analyzed in the frequency domain by decomposition into spectral components and then averaging over all ensembles. The averaged spectral components represent the mean square value of the acoustic pressure at a discrete frequency in the spectrum. From the mean square pressure a sound pressure level (SPL) spectrum was calculated referenced to 20 μPa. Minniti et al.[11] gave the uncertainty in facility SPL measurement to be ± 0.8 dB referenced to 20 μPa with 95% confidence.

Figure 9 shows far-field acoustic spectra at angular locations on the pressure and suction sides of the airfoil. The spectra show that the acoustic signals are dominated by the component at the rod passage frequency and its second, third, and fourth harmonics. Note the similarity between Figs. 9 and 6. The location and relative magnitudes of the peaks of the spectra are almost identical. This is intuitive because the unsteady velocities shown in Fig. 6 are ultimately responsible for the acoustic production through their interaction with the surface of the airfoil.

The directivity pattern of the acoustic field can be obtained by tracking the value of these peaks along the arcs made in the field by the microphone. Figure 10 tracks the first three peaks, denoted by the mode, or harmonic, number m of the acoustic spectra, with $m = 1$ corresponding to the fundamental rod passage frequency,

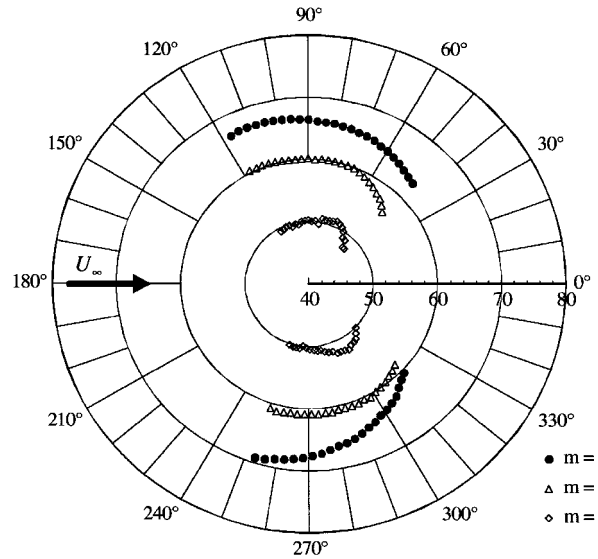

Fig. 10 Directivity of SPL produced by the airfoil for $M_\infty = 0.05$, $k_1^* = 3.0$, and $k_2^* \approx 4.5$.

$m = 2$ corresponding to the second harmonic, and so on. The background levels present without the airfoil in the flow were measured below 45 dB for all modes in all directions and, therefore, cannot be plotted on Fig. 10. The directivity pattern of the first mode resembles the radiation from a dipole source with some variation on the suction side of the airfoil where the fundamental harmonic is pushed upstream slightly. The second mode is more symmetric and resembles dipole radiation. However, the third mode shows a flattened pattern pushed downstream on both sides of the airfoil and appears to show quadrupole effects as observed by Atassi et al.[12] for airfoils of finite thickness in high-wave-number flow.

Unsteady Surface Pressure Measurements

The unsteady surface pressures on the airfoil were measured using thin-film, unsteady pressure transducers distributed along the chord as shown in Fig. 11. The airfoil was instrumented with a total of 14 pressure transducers at seven axial stations on the upper and lower surfaces of the airfoil. The pairs were concentrated toward the leading edge to investigate the pressure distribution near the area where theoretical methods predict a singularity. The distribution was also staggered so that those sensors near the leading edge would not trip the flow passing over downstream sensors.

The transducers were constructed from small disks of polyvinylidene fluoride (PVDF) piezoelectric film that enabled measurement of small unsteady pressure quantities without disturbing the flowfield by intrusive techniques. Dynamic calibration of the sensors

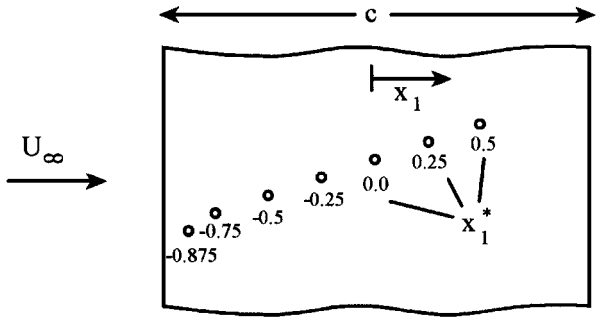

Fig. 11 Distribution of pressure transducers on airfoil with location as a fraction of half-chord x_1^* from the leading edge.

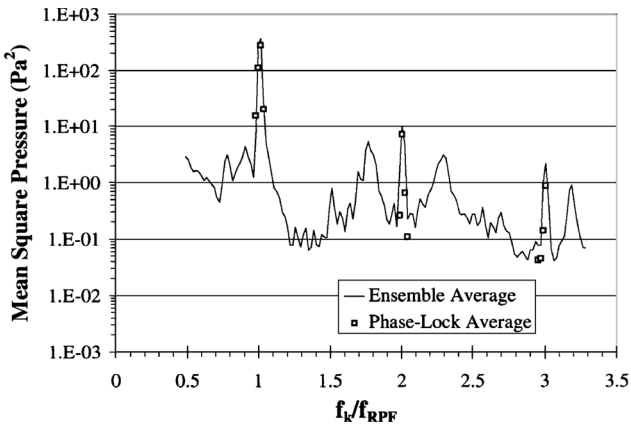

Fig. 12 Ensemble-averaged pressure spectra at pressure side leading-edge sensor, $x_1^* = -0.875$.

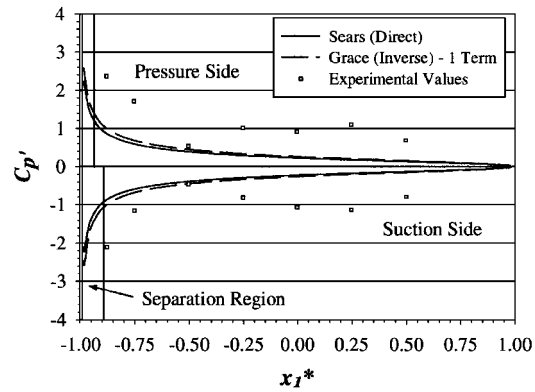

Fig. 13 Distribution of fundamental mode of unsteady pressure coefficient $C_{p'}$ on airfoil for $M_\infty = 0.05$, $k_1^* \approx 3.0$, and $k_2^* \approx 4.6$ compared with airfoil response defined using Refs. 1 and 2.

was accomplished by comparison of the sensor signal to a 0.635-cm (0.25-in.) B&K microphone when exposed to an acoustic signal broadcast from a loudspeaker. The signal broadcast was typically band-limited white noise or a sweeping sine wave that concentrated acoustic energy at discrete values over a small frequency range. Calculation of the ensemble-averaged, frequency-response function between the transducer and microphone completed calibration. To ensure accurate calibration, any frequency data gathered when the coherence between the transducer and microphone dropped below 0.98 were rejected as unreliable.

The frequency-response function gave the magnitude and phase of the output of the PVDF sensors relative to an equivalent output that would be obtained by the B&K microphone assuming it had a flat response over the frequency range of interest. The response functions measured for the sensors showed a low-frequency rolloff below 100 Hz with a region of flat response between 100 and 350 Hz. For the 14 sensors used in the experiment, the average sensitivity over the frequency range of interest (100–250 Hz) was found to be 85 Pa/V. Although the sensitivity of the individual sensors varied in overall magnitude by up to 20% of this value, the shape of the response function from sensor to sensor was very consistent. A phase lag of approximately 0.2π rad existed over the frequency range of interest between the sensor and B&K microphone. However, the lag did not vary more than $\pm 0.05\pi$ rad from sensor to sensor, allowing for accurate estimation of relative phase between sensors. The construction and calibration of the PVDF sensors are covered in greater detail in Ref. 13. Based on the results presented, the uncertainty of the unsteady pressure measured by the PVDF sensors was ±8% of the measured value with 95% confidence.

Figure 12 shows the comparison between an ensemble-averaged unsteady pressure spectrum and the components of the phase-lock-averaged spectrum associated the rod passage harmonics for the leading-edge sensor on the pressure side. Again, peaks at the gust frequency, the second and third harmonic, dominate the spectra. The broadband levels in the ensemble-averaged spectrum are not as well behaved as in the previous spectra of the velocity and acoustic measurements; however, these modes are produced by electrical and vibrational noise in the signals and should not be interpreted as flowfield phenomena.

By tracking the values associated with each of these peaks, the distribution of the unsteady pressure coefficient $C_{p'}$ along the airfoil chord was obtained. Figure 13 shows this distribution for the first peak in the power spectra compared with the two estimates obtained using the Sears method and the inversion technique of Grace et al.[2] The estimate made by Sears uses Eq. (7) and the velocity data presented previously. The Grace estimate was obtained using the acoustic data as an input to an inversion technique applied to Eq. (9). For incompressible flow, the solution depended on only a single term of the collocation technique used to complete the inverse process.

Good agreement was obtained between the two theoretical methods; however, only limited agreement was found with the experimental data. The experimental distribution showed much higher pressure than the theoretical developments over much of the airfoil chord. Flow visualization using oil and titanium dioxide spread on the airfoil indicated the presence of separation regions on both sides of the airfoil near the leading edge. These separation bubbles and the redeveloping boundary layers downstream of reattachment are at least partly responsible for the shape of the experimental distribution. However, despite the presence of these regions of high unsteady pressure, the acoustic radiation produced by the gust airfoil interaction was not significantly affected, as evidenced by the agreement between the two theoretical methods.

The experimental data of Fig. 13 indicate that the presence of this separation region has amplified the level of unsteady pressure measured near the leading edge. It is likely that the separation region would be driven into an oscillation at the gust frequency by the wake passage, which would account for the increase in unsteady pressures measured near the leading edge. Velocity measurements made in close proximity to the airfoil along the chord confirmed the presence of these separation regions and their effect of locally increasing the magnitude of the gust.

Further insight is obtained by analysis of the phase variation along the airfoil. Figure 14 shows the unsteady pressure phase associated with the fundamental harmonic measured relative to the first sensor station on the unsteady pressure side of the airfoil. According to the incompressible, inviscid development of Sears, the unsteady lift on the airfoil due to the change in angle of attack produced by the gust interacting with the leading edge should act instantaneously everywhere because the flow is potential. However, between the third and fifth stations on both sides of the airfoil, an increasing phase corresponding to convection with the mean flow is observed. This convection gives evidence of locally produced disturbances created by oscillation of the separation bubble being shed into the boundary layer. As these disturbances move downstream, they locally affect the unsteady pressure and dominate the phase distribution. However, as they dissipate, their local effect vanishes, and the instantaneous lift, predicted by Sears, again dominates the unsteady pressure on the aft portion of the airfoil.

Figure 15 shows the distribution of the unsteady pressure coefficient associated with the second harmonic of the spectra. For this

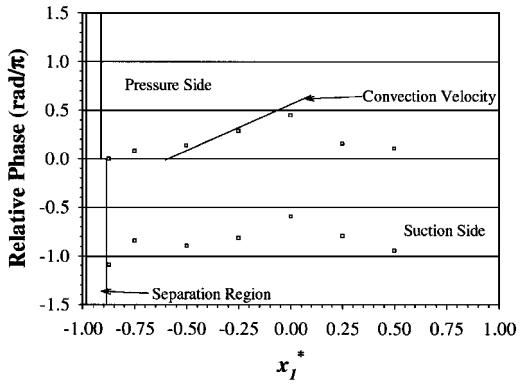

Fig. 14 Distribution of unsteady pressure phase of fundamental harmonic on airfoil for $M_\infty = 0.05$, $k_1^* \approx 3.0$, and $k_2^* \approx 4.6$, measured relative to sensor signal at the first measurement station on the unsteady pressure side of the airfoil.

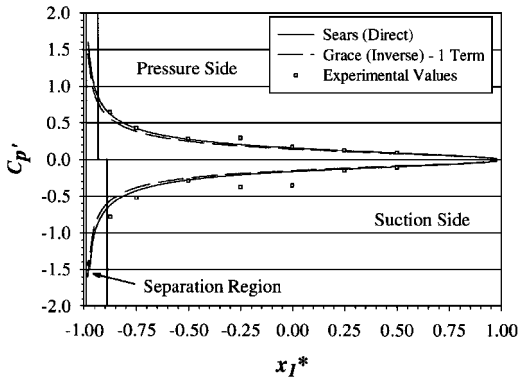

Fig. 15 Distribution of second harmonic of unsteady pressure coefficient $C_{p'}$ on airfoil for $M_\infty = 0.05$, $k_1^* \approx 6.0$, and $k_2^* \approx 9.2$ compared with airfoil response defined using Refs. 1 and 2.

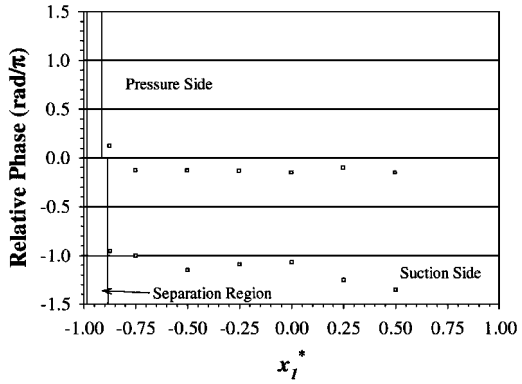

Fig. 16 Distribution of unsteady pressure phase of second harmonic on airfoil for $M_\infty = 0.05$, $k_1^* \approx 6.0$, and $k_2^* \approx 9.2$, measured relative to sensor signal at the first measurement station on the unsteady pressure side of the airfoil.

harmonic, good agreement with theoretical results and better agreement with experimental data were obtained along most of the airfoil chord. Near the leading edge, on the suction side of the airfoil, there was a slight relative increase in the experimental data, which indicated some viscous effects. However, by inspection of Fig. 16, the chordwise distribution of phase associated with this harmonic was much more constant, with only slight variations near the leading edge. On the suction side of the airfoil, some convection of information was indicated by phase variation at the first two stations, which again indicated viscous effects in this region. The effects of the separation region were limited to near the leading edge for the fundamental harmonic, and with their effect reduced in the second harmonic, good agreement was obtained with both theoretical methods.

Conclusions

The experimental configuration allowed for the description of all physical quantities associated with the unsteady problem, i.e., the unsteady velocity field, the unsteady pressure distribution on the airfoil, and the acoustic far field produced by the interaction between the airfoil and the unsteady flow. The description of the flow was accomplished by experimentally defining the gust amplitude components and reduced frequencies. The gusting was periodic and allowed for analytical treatment of the unsteady problem using individual frequency components of the signals. The acoustic production was defined by measuring the magnitude and directivity of the acoustic field over a large range of circumferential locations. In addition, the measurements characterized the phase variation of the acoustic response over the region of interest. The measurements were in good agreement with expected trends and agreed qualitatively with both the velocity and surface pressure measurements.

Finally, the distribution of unsteady pressure on the surface of the airfoil was established at seven chordwise stations for the fundamental and second harmonics. These data displayed trends that were in agreement with qualitative observations from both the velocity fields and the acoustic fields. The pressure distributions were compared with estimates given by the Sears[1] method for an ideal flat plate used with the measured unsteady flow quantities. Additionally, the inverse technique developed by Grace et al.[2] for use on ideal flat plates provided another estimate of the pressure distributions using the acoustic data as input. This method accurately reproduced the solution of Sears, which, if taken a step further, indicates that accurate reproduction of the unsteady flow quantities could be recovered.

Only limited agreement between the theoretical results and the experimental data was obtained at the fundamental rod passage frequency. Viscous effects, such as the leading-edge separation regions and their effect on the boundary layer downstream of reattachment, which are not included in the theoretical developments, are the principal reason for the disagreement. Better agreement was obtained at higher values of reduced frequency, where the viscous effects of separation were much smaller. The results show the importance of viscous effects in establishing the unsteady pressure distribution along the airfoil. However, although the effect on the unsteady pressure is significant, the acoustic radiation is much less sensitive to viscous effects produced locally on the surface.

Acknowledgments

This research was performed at the Hessert Center for Aerospace Research, Department of Aerospace and Mechanical Engineering, University of Notre Dame, for the U.S. Navy, Office of Naval Research, Arlington, Virginia, under Contract N00014-95-1-0488. The authors would like to thank the Program Manager, Lawrence P. Purtell, and William Blake of the U.S. Naval Surface Warfare Center, Carderock Division, for their comments at various stages of this research.

References

[1] Sears, W. R., "Some Aspects of Non-Stationary Theory and Its Practical Application," *Journal of the Aeronautical Sciences*, Vol. 8, No. 3, 1941, pp. 104–108.

[2] Grace, S. P., Atassi, H. M., and Blake, W. K., "Inverse Aeroacoustic Problem for a Streamlined Body Part 1: Basic Formulation," *AIAA Journal*, Vol. 34, No. 11, 1996, pp. 2233–2240.

[3] Von Kármán, T., and Sears, W. R., "Airfoil Theory for Non-Uniform Motion," *Journal of the Aerospace Sciences*, Vol. 5, No. 10, 1938, pp. 379–390.

[4] Atassi, H. M., "The Sears Problem for a Lifting Airfoil Revisited—New Results," *Journal of Fluid Mechanics*, Vol. 141, 1984, pp. 109–122.

[5] Atassi, H. M., Fang, J., and Patrick, S. M., "Direct Calculation of Sound Radiated from Bodies in Non-Uniform Flows," *Journal of Fluids Engineering*, Vol. 115, No. 4, 1993, pp. 573–579.

[6] Atassi, H. M., and Dusey, M. P., "Acoustic Radiation from a Thin Airfoil in Nonuniform Subsonic Flow," AIAA Paper 90-3910, Oct. 1990.

[7] Fujita, H., and Kovasnay, L. S. G., "Unsteady Lift and Radiated Sound from a Wake Cutting Airfoil," *AIAA Journal*, Vol. 12, No. 9, 1974, pp. 1216–1221.

[8] Mueller, T. J., Scharpf, D. F., Batill, S. M., Strebinger, R. B., Sullivan, C. J., and Subramanian, S., "The Design of a Low-Noise, Low-Turbulence Wind Tunnel for Acoustic Measurements," AIAA Paper 92-3883, July 1992.

[9]Scharpf, D. F., "An Experimental Investigation of the Sources of Propeller Noise Due to Turbulence Ingestion," Ph.D. Dissertation, Dept. of Aerospace and Mechanical Engineering, Univ. of Notre Dame, Notre Dame, IN, 1993.

[10]Minniti, R. J., III, "An Experimental Investigation of Thin Airfoils Exposed to Periodic Gusting Including the Inverse Aeroacoustic Problem," Ph.D. Dissertation, Dept. of Aerospace and Mechanical Engineering, Univ. of Notre Dame, Notre Dame, IN, 1997.

[11]Minniti, R. J., III, Batill, S. M., and Mueller, T. J., "Experimental Uncertainty of Sound Pressure Level Measurements Made in a Free-Jet Anechoic Wind Tunnel Facility," *Proceedings of First Joint CEAS/AIAA Aeroacoustics Conference*, Vol. 2, German Society for Aeronautics and Astronautics, Bonn, Germany, 1995, pp. 1105–1114 (CEAS/AIAA Paper 95-151).

[12]Atassi, H. M., Subramaniam, S., and Scott, J. R., "Acoustic Radiation from Lifting Airfoils in Compressible Subsonic Flow," AIAA Paper 90-3911, Oct. 1990.

[13]Mueller, T. J., Sullivan, C. J., and Minniti, R. J., III, "A Thin Film Sensor for the Measurement of Unsteady Pressure on Propellers and Other Aerodynamic Surfaces," *Proceedings of the Royal Aeronautical Society's Wind Tunnel and Wind Tunnel Test Techniques* (Cambridge, England, UK), Royal Aeronautical Society, London, 1997, pp. 32.1–32.8; also *Aeronautical Journal of the Royal Aeronautical Society* (to be published).

S. Glegg
Associate Editor